Fluid Equilibrium

Material Computation in Ferrofluidic Castings

Zach Seibold
Material Processes + Systems Group, Harvard GSD

Jonathan Grinham
Harvard GSD

Olga Geletina
Harvard GSD

Onyemaechi Ahanotu
Wyss Institute, Harvard University

Allen Sayegh
Harvard GSD

James Weaver
Wyss Institute, Harvard University

Martin Bechthold
Material Processes +Systems Group, Harvard GSD

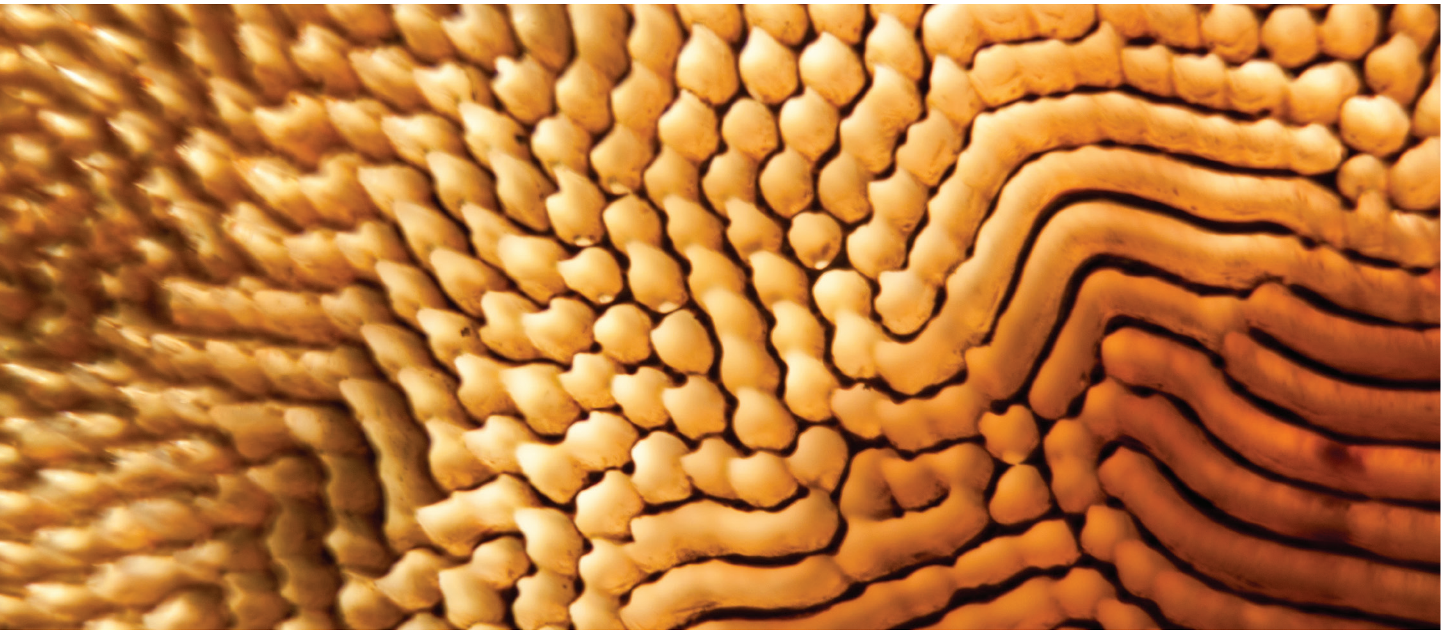

1 Detail image of ferro-tile cast in epoxy resin.

ABSTRACT

We present a computationally based manufacturing process that allows for variable pattern casting through the use of ferrofluid: a mixture of suspended magnetic nanoparticles in a carrier liquid. The capacity of ferrofluid to form intricate spike and labyrinthine packing structures from ferrohydrodynamic instabilities is well recognized in industry and popular science. In this paper we employ these instabilities as a mold for the direct casting of rigid materials with complex periodic features. Furthermore, using a bitmap-based computational workflow and an array of high-strength neodymium magnets with linear staging, we demonstrate the ability to program the macro-scale pattern formation by modulating the magnetic field density within a single cast. Using this approach, it is possible to program specific patterns in the resulting cast tiles at both the micro- and macro-scale and thus generate tiled arrays with predictable halftone-like image features. We demonstrate the efficacy of this approach for a variety of materials typically used in the architecture, engineering, and construction industries (AEC), including epoxys, ceramics, and cements.

INTRODUCTION

Magnetic fluids have fascinated scientists, commercial designers, and artists alike due to their ability to be manipulated, controlled, and shaped using magnetic fields. Typically referred to as ferrofluids, these liquids consist of a colloidal suspension of iron nanoparticles (NPs), most commonly magnetite (Fe_3O_4), in a carrier liquid such as oil, kerosene, or water. The small scale (<10 nm) and surfactant coating surrounding the iron NPs prevent the particles from settling and clumping, thus maintaining fluidity even under high magnetic field strengths (Rinaldi et al. 2005). When exposed to a magnetic field, ferrofluids form regular patterns of peaks and valleys. These patterns are the result of the Rosensweig instability (ferrofluid instability), which describes a minimum energy state between the magnetic field, gravity, and surface tension acting on the colloidal mixture (Cowley and Rosensweig 1967; Rosensweig 1997).

Since the development of ferrofluids in the 1960s, research has focused on the synthesis and functionalization of the NPs as well as the characterization of their surface properties. Early studies by Cowley and Rosensweig (1967) provided mathematical and experimental models to describe the formation of regular spikes in a hexagonal pattern (Rosensweig 1997; Rinaldi et al. 2005; Odenbach 2009). These models have since been expanded to include the use of finite element methods, and the full characterization of the patterns generated by ferrofluid instabilies are well documented in the scientific literature (Hansen and Mørup 1998). Furthermore, mathematical models have been developed to classify pattern instabilities (stripes, bubbles, chevrons, etc.) when a magnetic field is applied to ferrofluid and an immiscible nonmagnetic fluid in open pools (Boudouvis et al. 1987; Elias et al. 1997), and in the confinement of a Hele-Shaw cell, in which the ferrofluid and immiscible fluid are sandwiched between two planar surfaces (Rosensweig et al. 1983). A variation of this set-up includes a Hele-Shaw cell with in-plane rotation (Elborai et al. 2005).

Assisted by the decreased cost of production, the use of ferrofluids for commercial and research purposes has grown in scope. Applications include magnetic resonance imaging, sealings, bearings, shock absorbers, grinding, and polishing, and a sizable industry adoption for loudspeaker heat sinks (Rosensweig 1997; Rinaldi et al. 2005; Odenbach 2009). The homogeneous distribution of ferrofluid NPs has also been shown to control the microstructure design of anisotropic particles in slip-casting ceramics, metal, or polymer-functional matrices (Le Ferrand 2015), and in the use of direct ink-writing additive manufacturing processes (Kokkinis 2015).

Several artists and designers have employed the behavior of Rosensweig instabilities and labyrinthine patterns to generate unique visual effects. Two such examples include artist Sachiko Kodama, whose work has focused on the manipulation of ferrofluid across different geometric structures (sachikokodama.com) and Zelf Koelman, whose Digital FerroFluid Display suspends ferrofluid in a display manipulated by a grid of electromagnets to confer information, such as time, using a near-binary control of the magnetic field (Koelman et al. 2015). Both examples explore the aesthetic potential of the material in a dynamic state. Other notable instances include the work of Jólan van der Wiel (www.jolanvanderwiel.com) and Goldman and Myer's (2017) "Freezing the Field" project, which generate sculptural objects by adding iron filings to a casting medium. Here the artists use centimeter-scale iron particles, which form 3D chains and aggregates of multiple iron filings that affect the macroscopic properties of the mixtures, not the surface energy, as is the case for the colloid mixture of ferrofluid (Rinaldi et al. 2005).

In the past decade, scientific and architectural design research has focused on the ability to design or program material behavior across multiple length scales in order to generate novel form-finding processes and optimize material performance. This ability to program novel material behavior through changes in a material's geometry has been described as "material computation" within the field of architectural design (Menges 2012; Oxman 2012), or the production of "architected" or "meta-materials" within the engineering community (Fleck et al. 2010; Walser 2001).

In this paper, we introduce a novel manufacturing method that leverages the ability to program the unique formal effects achievable with ferrofluid in a nonmagnetic, immiscible fluid. We show that the dynamic patterns generated by the ferrofluidic instabilities can be molded in a range of castable materials by adapting methods first reported by Kisailus et al. (2013). Furthermore, by tuning the magnetic field generated by an array of neodymium (permanent) magnets using linear staging, we demonstrate that the formation of these patterns at multiple length scales and pattern types can be controlled computationally. As a result, our method can be used to generate halftone-like images in several castable materials using a bitmap-based digital workflow. This method can be applied to materials commonly employed in AEC industries to produce a range of products with forms and patterns that would be difficult or impossible to produce by other means. Lastly, the use of ferrofluid as a molding agent provides a near-net-shape casting process wherein the molding material, the ferrofluid, can be almost completely recovered and reused.

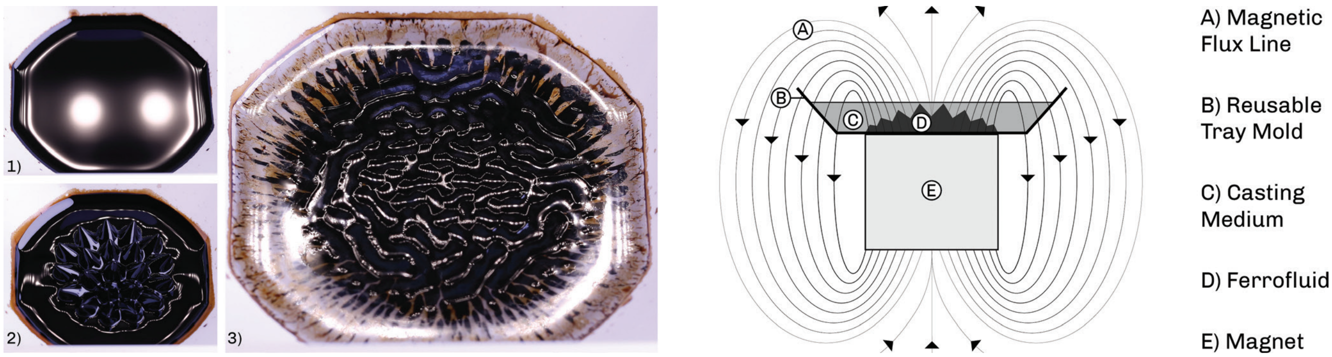

2

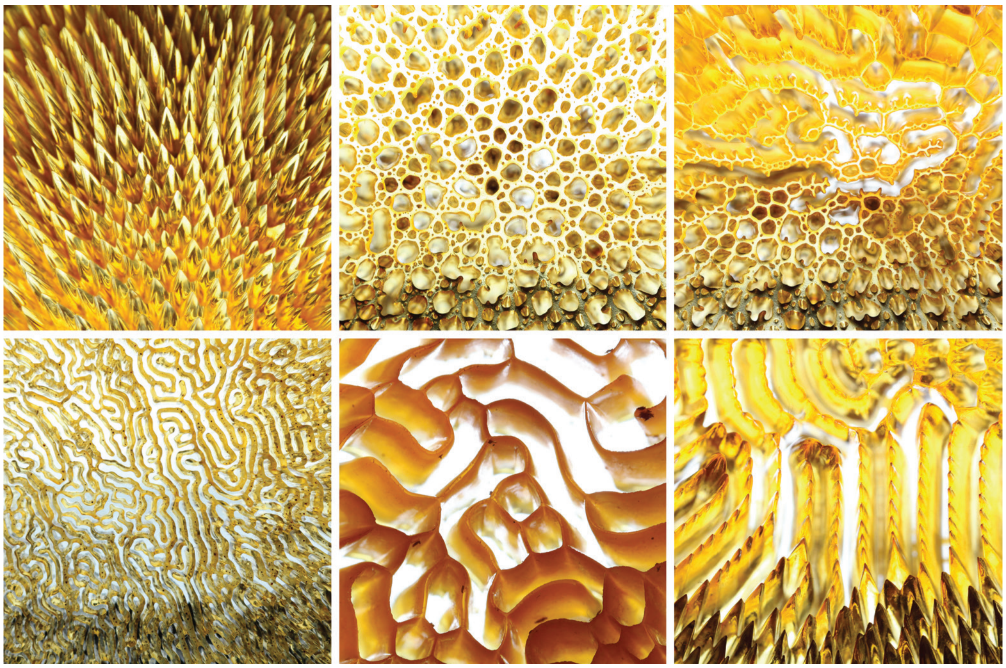

3

2 Left: 1) Ferrofluid without a magnetic field; 2) ferrofluid exposed to a magnetic field; 3) ferrofluid and uncured epoxy resin exposed to a magnetic field. Right: Diagram showing the fundamental components of casting process.

3 Detail images showing the range of patterns generated in epoxy resin by varying the magnetic field strength, quantity of ferrofluid, and amount of casting medium. Each image field shows a 30 mm square sample area.

4 Schematic diagram showing key components of the actuation mechanism. Magnets are shaded to indicate their relative positional values, from 18 mm (red) to 30 mm (green) below the casting surface.

This process thus presents an opportunity to generate form customization in cast components at the scale of the individual part, a prospect difficult or impossible to achieve using existing tooling strategies.

RESEARCH METHODS

Fundamental Principles

A general overview of the forces and material behaviors controlling the outcome of the manufacturing process described in this paper are as follows: Patterns cast using this approach are a result of a fluid equilibrium, a balance between gravitational, magnetic, and interfacial forces. Interfacial tension refers to the forces in a common boundary layer between two materials. In the case of the "unconfined" spikes (Figure 2.2), this is between ferrofluid and air, while in our casting-based work, it is between the ferrofluid and a casting medium (Figure 2.3).

The patterns formed by interfacial deformation are governed by the balance of attractive and repulsive forces (Seul and Andelman 1995). The ratio of repulsive to attractive force is referred to as the Bond number (N_b) of the system, and a system will self-organize if the Bond number is greater than 1. The primary attractive and repulsive forces in this system are gravitational, interfacial, and magnetic, with the summation of these forces equal to zero at equilibrium, as described in Equation 1 (Bourgine and Lesne 2010).

$$\Sigma F = F_g + F_m + F_s \qquad \text{(Equation 1)}$$

$$\Sigma F = 0 = \rho_f g a \lambda^2 + \mu_0 M^2 \lambda - \gamma_{f\text{-}m} a \qquad \text{(Equation 2)}$$

The expanded form of Equation 1 leads to Equation 2 (Bourgine and Lesne 2010), where ρ_f is the density of the ferrofluid, **g** is the gravitational constant, **a** is the interfacial area between the two fluids, **λ** is the wavelength of the instability, μ_0 is the magnetic susceptibility in a vacuum, **M** the magnetization of the ferrofluid from Currie's law, and $\gamma_{f\text{-}m}$ is the interfacial tension of the ferrofluid (**f**) and the immiscible medium (**m**). For a given ferrofluid, the only material properties that can be changed are the ferrofluid density and interfacial tension of the biphasic system. Simplifying Equation 2, and holding **M** constant, we find that for the same magnetization, we induce smaller wavelengths of instability as the interfacial tension decreases, yielding finer pattern features, such as a labyrinth formation, at lower magnetic fields (Equation 3). This makes intuitive sense when considering that the interfacial tension is a barrier to creating new interfacial contact between the two liquids. If that barrier or resistance to new interfaces is lower, then for the same magnetic field strength, the system will favor higher surface area patterns (from cones to flattened cones with tip instabilities, connected ridges, then deformed connected ridges). Similar to these unconfined systems, confinement of the pattern in the z dimension using a plate will lead to transitions from bubbles to stripes and more complex shapes within the biphasic system. A reaction diffusion analogue of this is observed in nature, leading to such patterns as zebra stripes and leopard spots.

$$\gamma_{f\text{-}m}=C_g\lambda^2+C_m(\lambda/a) \qquad \text{(Equation 3)}$$

For design considerations, the capillary length is defined as $\lambda_s=\sqrt{(\gamma_{f\text{-}m}/\rho g)}$, and as the interfacial tension decreases, the capillary length also decreases. For all else being equal, water containing patterning media (ceramics) would have a higher interfacial tension compared to the more hydrocarbon-dominant materials (epoxies), leading to larger capillary lengths for ceramics and creating larger minimum features for similar applied magnetic fields.

Casting Process

In the current process, we adapt the casting methods first described by Kisailus et al. (2013), which exploit the patterns generated by the shape instability of the ferrofluid and a nonmagnetic immiscible fluid. By first placing ferrofluid within a magnetic field, and then pouring a casting material around the spike formations, we can generate a predictable and controlled molding template with highly ordered structures based on the ferrodynamic instabilities as described previously (Figure 2).

By varying the amount of ferrofluid, casting material, and magnetic field strength, a wide range of multi-scale patterns are possible, including but not limited to honeycombs, grids, labyrinths, spikes, and ridges (Figure 3). After the casting material has cured, the magnetic field can be removed, restoring the ferrofluid to an unstructured liquid state, thus effectively removing the molding template. Post removal, the solidified casting material is washed with kerosene to clean the surface and remove any residual

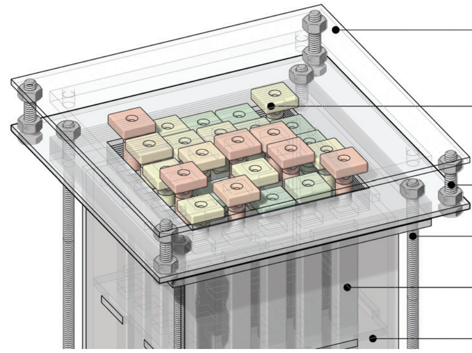

4

ferrofluid. When compared with existing molding and manufacturing methods, this approach allows for submillimeter, high-aspect-ratio, and tortuous structures; lower tooling and equipment costs; higher scalability; and greater variation of possible patterns (Kisailus et al. 2013).

Description of Actuator

We explored several means of generating and manipulating a variable magnetic field in a repeatable, reliable fashion. Commercially available electromagnets produced undesirable ring or bubble-shaped pattern formations in ferrofluid, while bespoke electromagnets were unable to generate a sufficient field strength. Early tests with fixed arrays of neodymium magnets, in contrast, achieved promising results. Based on these initial findings, the primary actuation mechanism developed for this study produces a variable magnetic field via direct positional control of twenty-five 13,200 gauss neodymium magnets (Figure 4).

The mechanism consists of a 5 x 5 array of neodymium block magnets. The vertical position of each magnet is controlled by a dedicated linear actuator. The extension of each actuator, and thus the position of each magnet, can be controlled individually to produce various field conditions within the array. A clear acrylic platform, 7 mm (0.28″) in thickness, located above the magnets, provides a flat surface for the placement of casting molds (Figure 5).

Early tests employed hall effect sensors to measure the relative strength of a magnetic field and verify the accuracy of relying on the physical measurement of magnet position to determine field strength. Placing a magnet closer to the mold resulted in a higher concentration of ferrofluid above the magnet. Testing revealed that a distance range of 18–30 ± 1.5 mm (0.71″–1.18″) from the top surface of the platform provided the greatest control of the ferrofluid. At distances greater than 30 mm (1.18″) from the top of the platform, field strength was insufficient to produce prominent features in the ferrofluid and casting medium. Conversely, at distances less than 18 mm (0.71″), the field

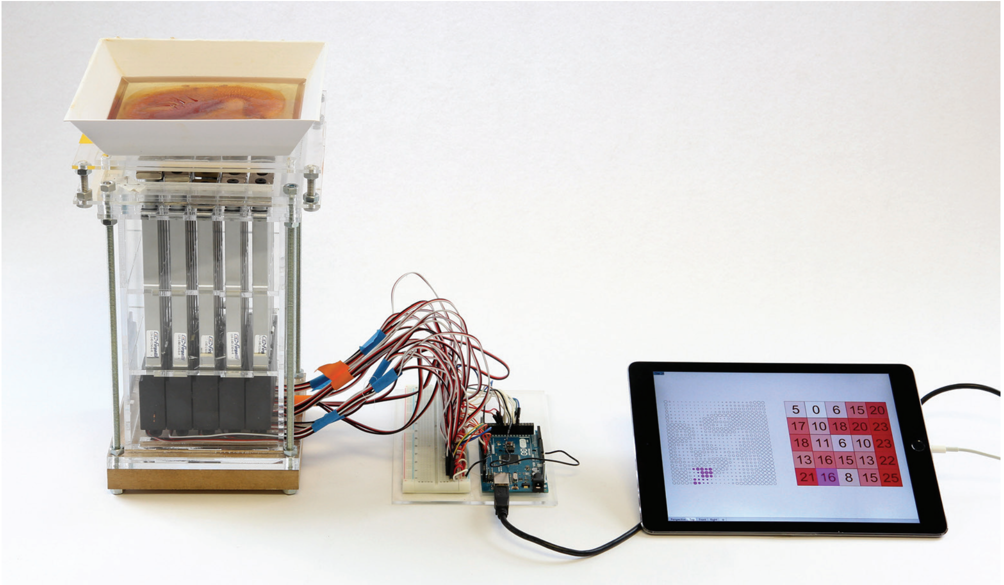

5

5 Photograph of the actuator assembly with an epoxy cast tile on the upper platform (left), the Arduino microcontroller and circuit (middle), and the digital interface developed in Grasshopper for Rhinoceros 5.0 (right).

6 Diagram showing the range of image processing and pattern calibration strategies developed.

become too concentrated and would produce discontinuous groupings. Each actuator could be set to a range of 11 fixed positional values within this distance range.

Digital Workflow

A digital interface was developed to control the position of each actuator in real time. The user interface, comprised of a custom definition in the Grasshopper 3D plugin for Rhinoceros 5.0, synthesizes visual parameters with individual actuator positions and propagates the position values to an Arduino microcontroller. Positional values for the grid of actuators were generated from the tonal values of a given image. Conversion of the tonal values of an image into positional data for the linear actuators involved the following steps: An image was broken down into a square array of tiles, corresponding to the number of tiles to be cast. Each tile was then divided into a 5 x 5 grid, representing the area of the image that corresponded to each actuator. Each area within this 5 x 5 grid was further subdivided into a 5 x 5 array of points on the image. The tonal value of each of these 25 points was averaged to obtain a single value, which was then used to set the position of the corresponding actuator (Figure 6C). The relative tonal value of each tile was mapped to a range of ferrofluid quantities and determined the amount of ferrofluid required in each tile (Figure 6D).

TESTING AND PRODUCTION

To avoid the computational complexity of modeling the material interactions within the casting system, and to limit the number of physical studies required for validating such predictions, several simulation strategies were employed to predict the outcome of the casting process. These strategies, which borrow representational techniques from reprography and photography, facilitate rapid approximation of the casting process, enabling the verification of design parameters without the computational simulation of ferrofluid patterns or the physical production of casts.

Pattern Calibration: Halftone Representation

To understand the size of tile array required to effectively convey a given image, we employed a simulation method based on the reprographic technique of halftoning. This process involves the simulation of a continuous-tone image through the variable sizing or spacing of an array of dots (Figure 6B). In ferrofluidic casting, the diameter of a dot corresponded to the z-position of a single magnet, and thus diagrammed the field strength concentration for a given tile. A single image could be quickly discretized into an array of halftone tiles, providing a schematic understanding of the range of patterns and tonal values achievable with the system, as well as an indication of the resolution at which the discrete halftone dots appear to blend into a continuous image. In practical terms, this technique affords a strategy to predict the coarsest resolution required to create a recognizable image from an array of cast tiles.

Physical Simulation Method: Stop-Motion Photographs

We employed stop-motion photography to verify the correlation between the halftone tile diagramming strategy described in Section 3.1 and the patterning produced by ferrofluid when immersed in a casting material and exposed to a given magnetic field (Figure 6E). The simulation process is as follows: A styrene mold containing epoxy resin is placed on top of the actuation mechanism described previously. During the pot life of the resin, the

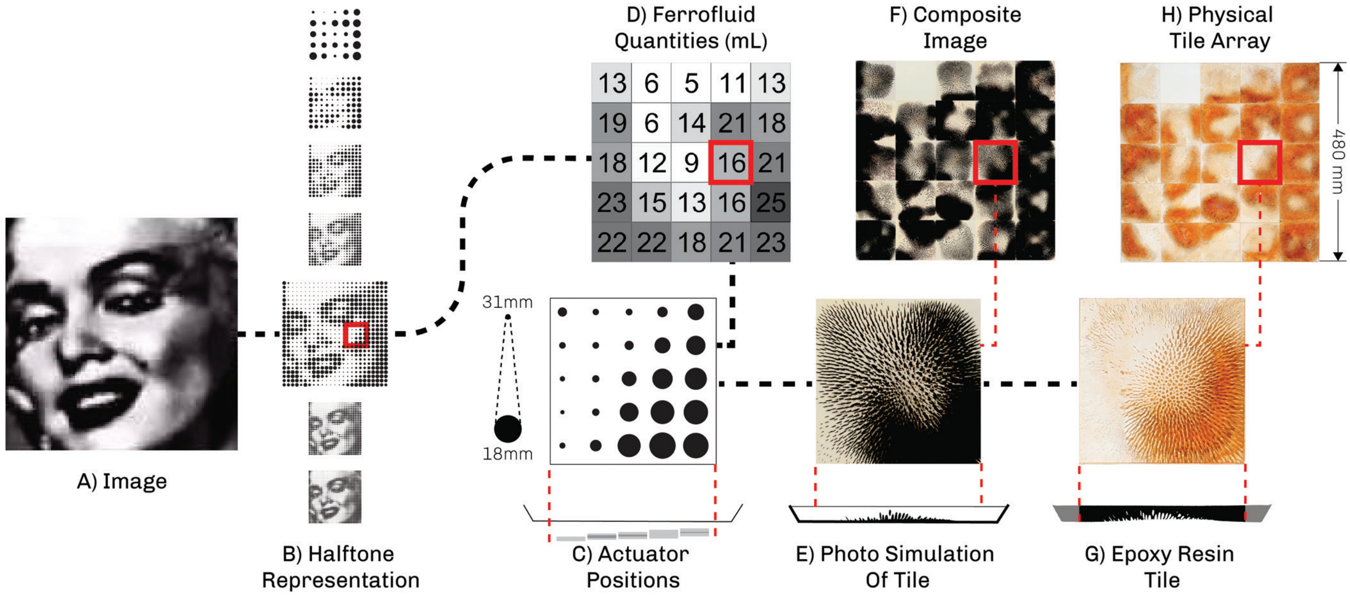

6

actuator is cycled through the array of tiles required for an image, in ascending order of tonal value. Ferrofluid is incrementally added to the casting matrix, corresponding to the tonal value of the associated tile. Once the quantity of ferrofluid and the position of the actuators are set, the cast is photographed perpendicular to its casting surface. The process is repeated until a representation of each tile in the array has been photographed.

Cycle time between photographs is determined by the hysteresis exhibited by the mixture of ferrofluid and the epoxy resin. In our experiment, a cycle time of approximately 10 seconds proved to be sufficient for the casting mixture to achieve equilibrium. The completed array of photographs is then assembled in a grid reflecting the organization of the original image (Figure 6F). These tests determined that there is a near-linear correlation between the amount of ferrofluid in each tile and the relative tonal value of the tile. Experiments with cropping the array of images also revealed the ideal tile size for assembling a completed image.

Unfortunately, the simulation technique described above is not without limitations. It is only applicable to translucent or transparent casting media such as epoxy resins, which can be imaged from above. Additionally, the opaque nature of the ferrofluid precludes the observation of the micro-scale patterning achievable with the casting process in regions of high ferrofluid density (which appear as solid black). By providing a macro-scale understanding of the patterning for each tile, however, the system demonstrates a reliable method of predicting the outcome of an array of casts before their physical production. Future process modifications could include the replacement of an opaque material with a transparent or translucent material with similar interfacial tension, providing a means of more easily observing and evaluating interior features.

Cast Tile Array

To test the validity of the diagrammatic and photographic simulations, an array of 25 casts was produced to represent a single image (Figure 7). The casts were made using 225 mL of epoxy resin and up to 25 mL of ferrofluid per tile. This quantity and ratio of ferrofluid to casting medium allowed for a range of patterns that was further informed by the individual magnet positions. Decreasing the thickness of the tile resulted in discontinuities and breakage in the cast materials, while increasing the thickness precluded the formation of labyrinthine patterns. Initial casts measured 132 mm per side, but were later trimmed to 96 mm. Producing tiles in a mold larger than the magnetic array limited the impact of the mold on ferromagnetic pattern geometry, and facilitated pattern continuity between individual casts. The patterning of the tile array (Figures 6H and 7) closely aligns with the results of the halftone representation (Figure 6B) and photographic simulation (Figure 6F).

Expanding Casting Method to Other Materials

Additional experiments were conducted on six other materials: gypsum cement, self-drying gypsum cement, hydraulic cement, terracotta, porcelain, and stoneware, with the goal of adapting the production process to a larger range of materials typically used in the AEC and other industries (Figure 8). The results show that across each material type, macro- and micro-scale patterns can be cast

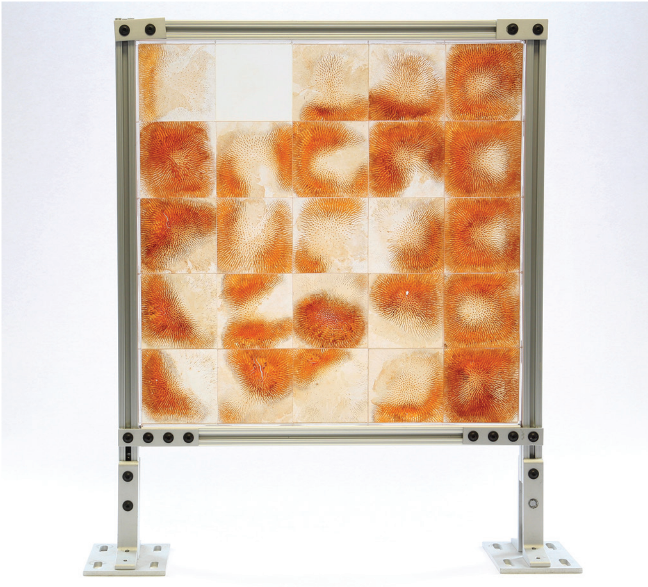

7 Photograph of epoxy resin tile array. Each tile measures 96 mm in width and height, used 225 g of resin, and up to 25 g of ferrofluid, resulting in a tile thickness of approximately 10 mm.

into these materials. However, the varied curing processes of the different compounds required material-specific modifications to the casting process (Table 1).

Table 1: Material parameters used in the casting process

Material	Material Volume (mL)	Ferrofluid Volume (mL)	Time in Mold (Appx.)
Epoxy Resin	100–225	0–25	5 hr +
Cements (Var.)	100–225	0–25	25 min
Terracotta	100–150	0–5	30 min
Porcelain	100–150	0–5	1 hr
Stoneware	100–150	0–5	40 min

The most significant process modifications were required for clay bodies, which shrank during the curing process (in addition to shrinking during firing), making them more susceptible to cracking. Thus, for the clay bodies, the mold, quantities of ferrofluid, and clay (1 mL and 100 mL, respectively), as well as the demolding times, were amended. Since atmospheric drying of the clay took prohibitively long (9–13 hours), gauze backing was placed on top of the open mold in direct contact with the ceramic body, and the mold was augmented with a plaster lid. The gauze and plaster lid helped wick water from the casts, appreciably reducing curing time (in excess of 9x) and increasing yield. The gauze layer also served as a structural backing for the tile and assisted the demolding process. The use of a more viscous release agent, such as castor oil, was also found to be beneficial.

DISCUSSION AND FUTURE RESEARCH

Process Modifications and Future Casting Workflow

Modifications to the actuation mechanism could expand the catalog of forms achievable with this system. A larger actuator, both in terms of the dimensions and resolution of the array, would reduce the number of elements required to cover a given surface. In addition, multiple orientations of magnets, such as a cubic or opposing parallel configuration, could expand the catalog of forms achievable with this system, moving away from a surface cladding toward a more spatially performative element. As described in the introduction, repeatable patterns can be generated within a Hele-Shaw cell, and as such, the process presented here may allow for the casting of complex labyrinth patterns or sandwiched composite material assemblies where the surfaces that define the boundary of the mold remain bonded to the resin. Furthermore, the use of immiscible fluids cured by means other than air, such as ultraviolet light or heat, could facilitate a more continuous production process and produce objects that are larger than the size of a given magnetic field.

Pattern Analysis

To quantitatively assess visual differences between the various casting materials and the corresponding patterns, epoxy resin, gypsum cement, and hydraulic cement casts were scanned using X-ray microcomputed tomography. The results of this process yielded a 3D model of the individual casts as well as snapshots of the tile topography in the X-Y plane at specific locations along the z-axis (Figure 9B, 9C). Using these individual z-slices, fast Fourier transform (FFT) analysis can be employed as an indicator of short- and long-range periodicity within the samples (Figure 9D). In the future, FFT can provide insight into spatial frequency, magnitude, and phase of the patterns generated in each material type. For example, our preliminary results demonstrate that the cast resin samples have higher frequency features. The gypsum cement and hydraulic cement samples, in contrast, exhibit a lower frequency pattern that spreads across a range of values corresponding to larger, more heterogeneous ferrofluid imprints; predicted by the equilibrium physics described in the Fundamental Principles subheading (Figures 9.1–9.3). Additional assessment of visual attributes may include fractal and medial axial analysis to correlate pattern formation to a particular casting medium. This data can in turn help further guide the computational model to achieve greater control over the structural and visual parameters of the final cast.

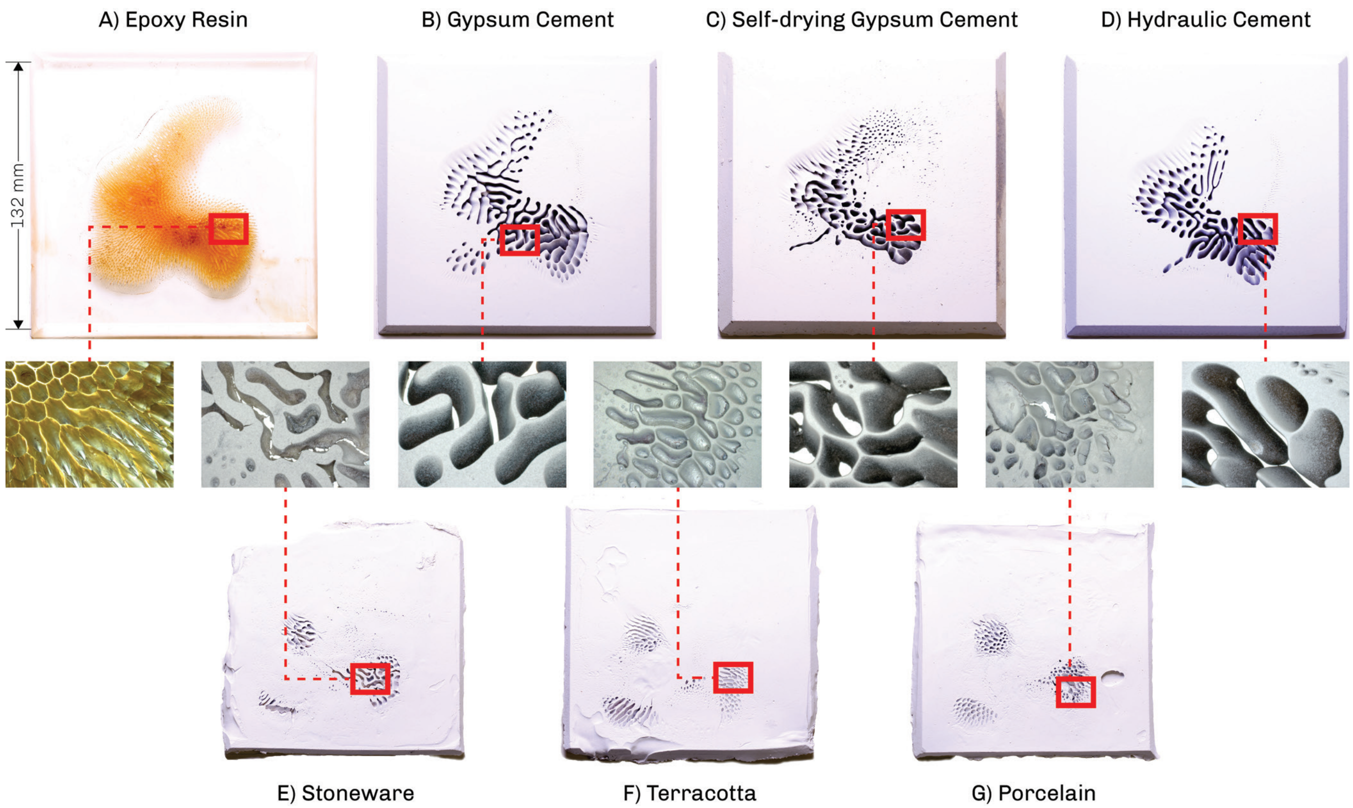

8 Tile casts generated in a range of materials using the same magnetic field. Tiles B–G were spray-painted white to facilitate comparison between pattern geometries, since remnant ferrofluid can cause staining or discoloration in untreated samples.

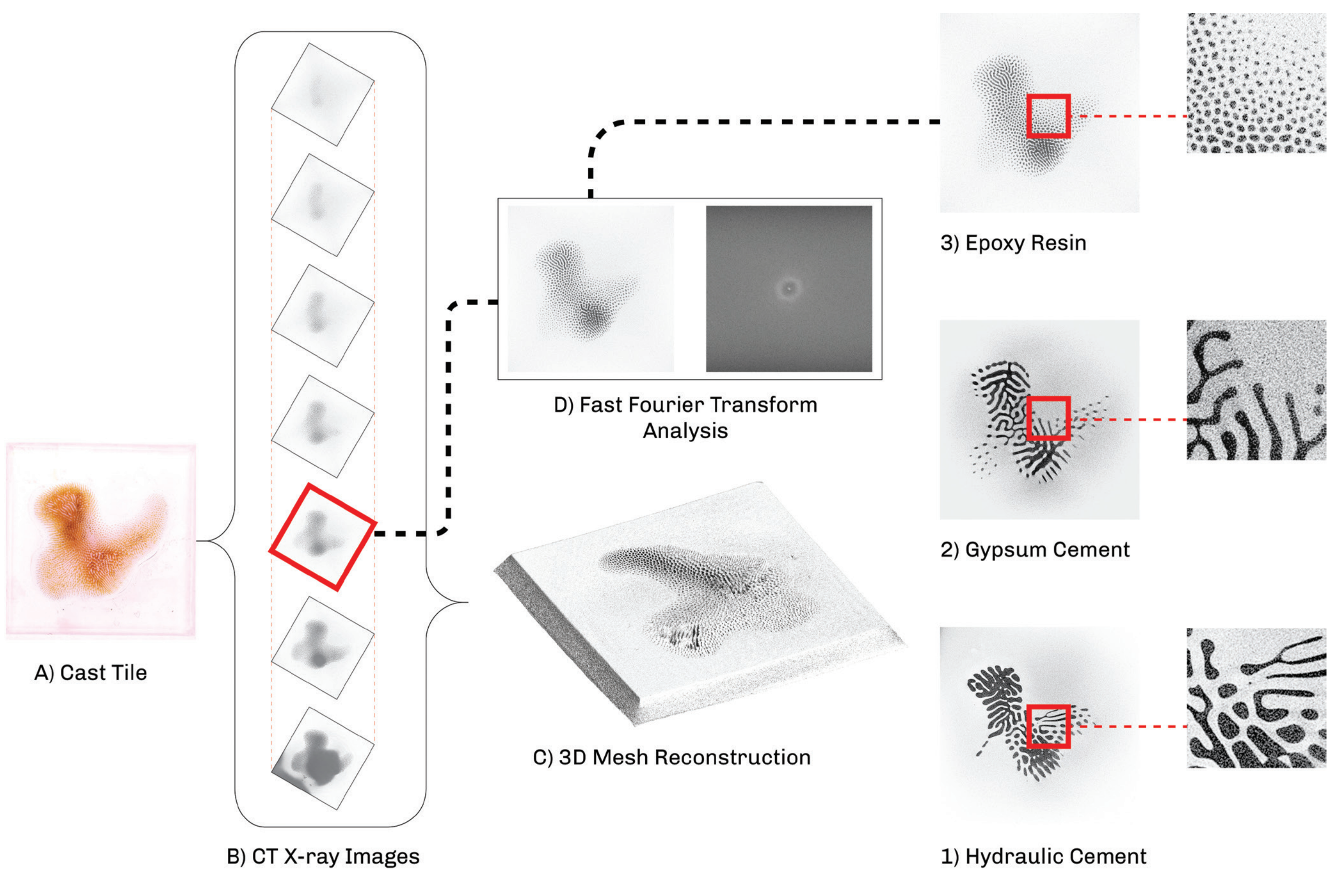

9 Pattern analysis using a combination of X-ray microcomputed tomography and FFT on the ferrofluid casts.

CONCLUSION

The current report presents a novel design and manufacturing workflow for variable pattern casting, with a particular focus on the use of ferromagnetic fluids as molding templates. Repeatable and predictable patterns are generated through the manipulation of magnetic field density via a custom actuation mechanism with multiple configurable magnetic "dies." The mechanism is positioned through an iterative feedback loop that relies on photographic images, which allows for desirable grayscale effects to be generated with ferrofluidic castings such that recognizable images can be produced in tiled arrays of cast modules. Future work will investigate optimizing the control of these magnetic dies through machine learning techniques. The casting process is applied to several materials commonly used in the AEC industries, including epoxy resins, ceramics, and cements. In comparison to existing casting methods, the process described here can produce variable parts with a range of intricate patterns with limited additional process materials or expense. This work thus constitutes a promising development in the design and manufacture of castable materials, enabling the implementation of a cost-effective means of element customization, and suggests a broader range of applications and design opportunities.

APPENDIX: EXPERIMENT SETUP

Tests described in this research used EFH1 Ferrofluid, a product manufactured by Ferrotec (Saturation Magnetization 440 Gauss, Viscosity @ 27c 6cP). Magnets utilized in the actuator are made of a grade N42 neodymium, iron, and boron magnetic alloy blend, and measure 19 mm (0.75˝) in length, 19 mm (0.75˝) in width, and 6.4 mm (0.25˝) in thickness. The gauss rating per magnet is 13,200 gauss. Pulling force per magnet is rated at 19.5 lbs. Magnets are actuated using Firgelli L16-140 linear actuators. Manufacturers of the casting media described in this research are as follows: epoxy resin (Aeromarine Products Epoxy Resin #300 + Noncycloaliphatic Epoxy Hardner #21), gypsum cement (Hydrostone), self-drying gypsum cement (Drystone), hydraulic cement (Rockite). The micro-computed tomography data were acquired with an XRA-002 X-Tek MicroCT (Xtek Inc., Cincinnati, OH). The 3D reconstructions were performed using CT-Pro (Nikon Metrology Inc., Brighton, MI), surface renderings were generated using VGStudio Max (Volume Graphics GmbH, Heidelberg, Germany). Fast Fourier transform studies were done using Python with NumPy and OpenCV libraries.

ACKNOWLEDGEMENTS

Research by the Material Processes and Systems (MaP+S) Group at the Harvard University Graduate School of Design, as part of the Adaptive Living Environments (ALivE) project in collaboration with the Wyss Institute for Biologically Inspired Engineering. Puja Patel and Kurt Fischer contributed to early process studies. This work was performed in part at Harvard University's Center for Nanoscale Systems (CNS), a member of the National Nanotechnology Infrastructure Network (NNIN), which is supported by the National Science Foundation under NSF award no. ECS-0335765.

REFERENCES

Bourgine, P. and A. Lesne, eds. 2010. *Morphogenesis: Origins of Patterns and Shapes.* Cham, Switzerland: Springer.

Boudouvis, A., J.L. Puchalla, L.E. Scriven, and R.E. Rosensweig. 1987. "Normal Field Instability and Patterns in Pools of Ferrofluid." *Journal of Magnetism and Magnetic Materials* 65 (2): 307–10.

Cowley, M., and R. Rosensweig. 1967. "The Interfacial Stability of a Ferromagnetic Fluid. *Journal of Fluid Mechanics* 30 (4): 671–88.

Elborai, S., D.K. Kim, X. He, S.H. Lee, S. Rhodes, and M. Zahn. 2005. "Self- forming, quasi-two-dimensional, magnetic-fluid patterns with applied in-plane-rotating and dc-axial magnetic fields." *Journal of Applied Physics* 97 (10): 10Q303.

Elias, F., C. Flament, J. Bacri, and S. Neveu. 1997. "Macro-organized patterns in ferrofluid layer: Experimental studies." *Journal De Physique I* 7 (5): 711–28.

Fleck, N.A., V.S. Deshpande, and M.F. Ashby. 2010. "Micro-architectured materials: past, present and future." *Proceedings of the Royal Society of London A: Mathematical, Physical and Engineering Sciences* 466 (2121): 2495–516.

Goldman, M., and C. Myers. 2017. "Freezing the Field: Robotic Extrusion Techniques Using Magnetic Fields." In *Disciplines & Disruption: Proceedings of the 37th Annual Conference of the Association for Computer Aided Design in Architecture*, edited by T. Nagakura, S. Tibbits, M. Ibanez, and C. Mueller, 260–65. Cambridge, MA: ACADIA.

Hansen, M.F., and S. Mørup. 1998. "Models for the dynamics of interacting magnetic nanoparticles." *Journal of Magnetism and Magnetic Materials* 184 (3): L262–74.

Kisailus, D., J. Weaver, and G. Milliron. 2013. Magnetically Controlled Casting Process for Multistructural Materials. US Patent 20160151939A1, filed Feb. 14, 2013.

Kodama, Sachiko. "Sachiko Kodama's Portfolio." http://sachikokodama.com/en/w

Koelman, Z., M.J.d. Graaf, and H.J. Leeuw. 2015. "From Meaning to Liquid Matters." In *Proceedings of the 21st International Symposium on Electronic Art*, edited by Kate Armstrong. Vancouver, BC: ISEA.